Electronic Supplementary Information

Rational design of covalently bridged $[Fe^{III}_2M^{II}O]$ clusters

Pablo Alborés[†, §] * and Eva Rentschler[†]*

† Institute of Inorganic and Analytical Chemistry, Johannes Gutenberg - University of Mainz, Duesbergweg 10-14, D-55128 Mainz, Germany

Fax: +49 6131 / 39-23922

§ Departamento de Química Inorgánica, Analítica y Química Física, INQUIMAE (CONICET), Facultad de Ciencias Exactas y Naturales Universidad de Buenos Aires, Pabellón 2, Ciudad Universitaria, C1428EHA Buenos Aires, Argentina

Fax: +5411 / 4576-3341

E-mail: albores@qi.fcen.uba.ar ; rentschl@uni-mainz.de

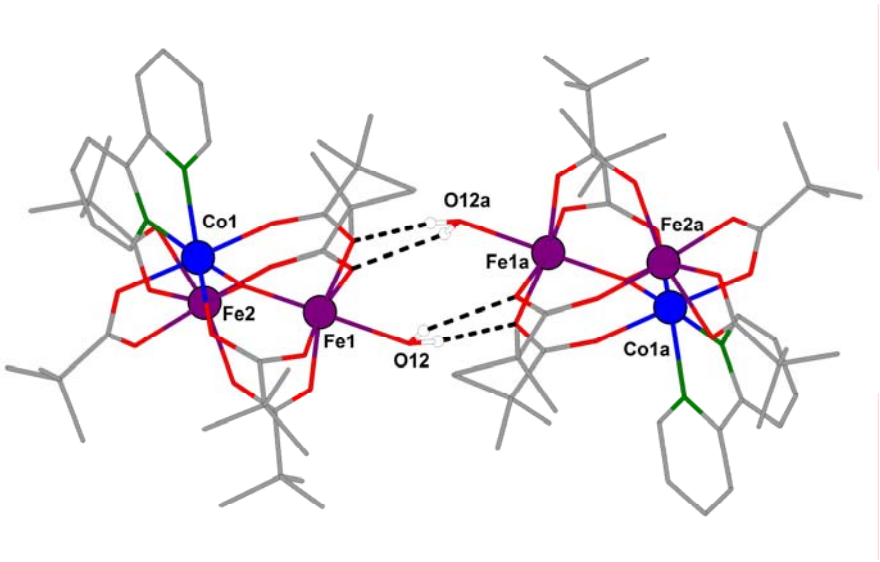

Figure S1. Molecular representation of the H-bonding between adjacent molecules in complex **1**. H atoms omitted for sake of clarity.

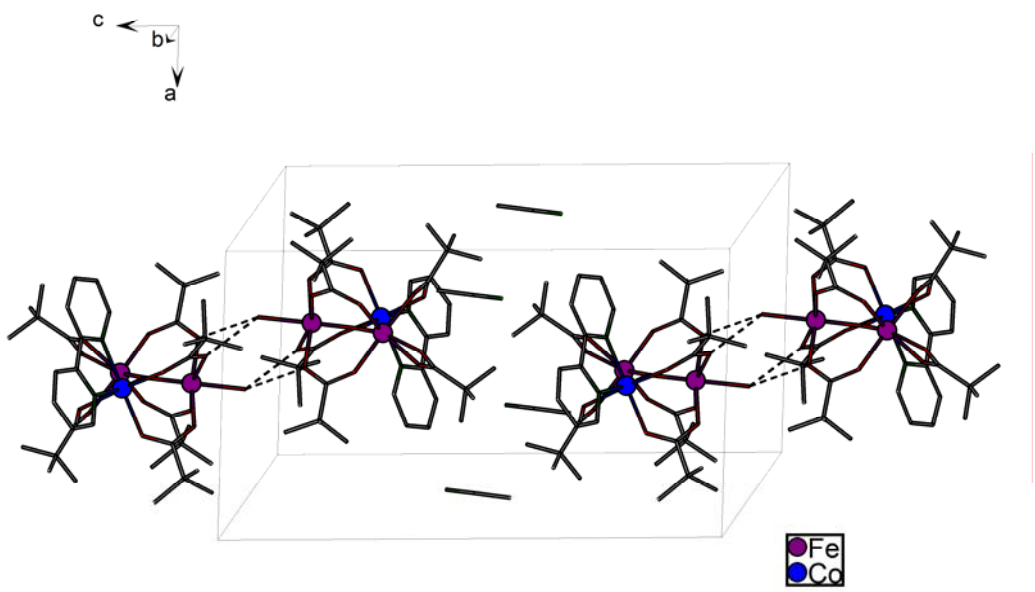

Figure S2. Arrangement of the H-bond interacting complexes in the crystal packing of **1**. H atoms omitted for sake of clarity.

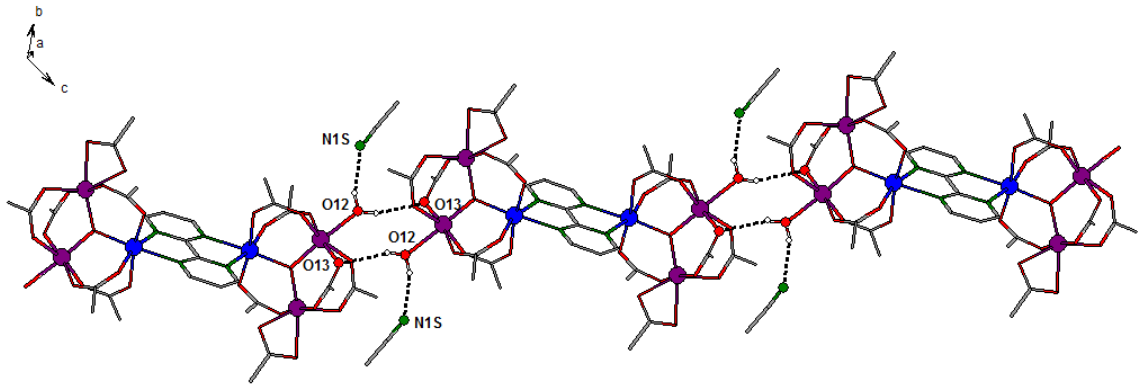

Figure S3. Molecular representation of the extended H-bond interaction in complex **4**. Blue: cobalt atoms, purple: iron atoms. H atoms and *tert*-butyl groups omitted for sake of clarity.

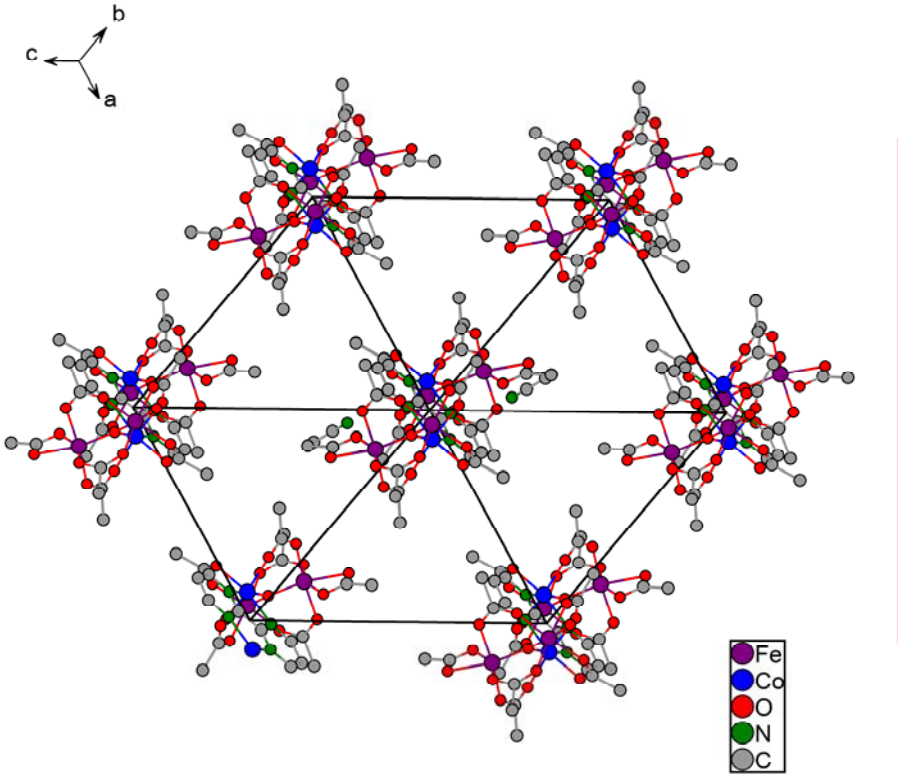

Figure S4. Crystal packing of the unit cell of complex **4**. View along the H-interacting chains. H atoms and *tert*-butyl groups omitted for sake of clarity.

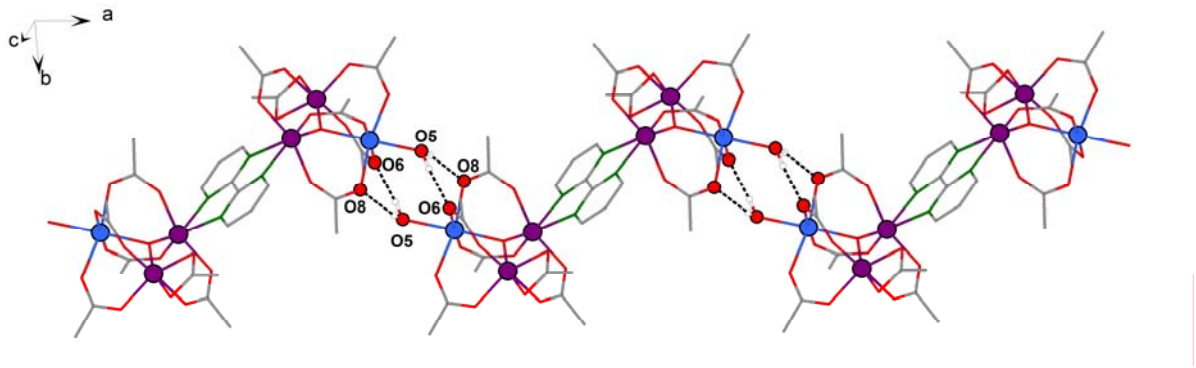

Figure S5. Molecular representation of the extended H-bond interaction in complex **6**. Blue: manganese atoms, purple: iron atoms. H atoms and *tert*-butyl groups omitted for sake of clarity.

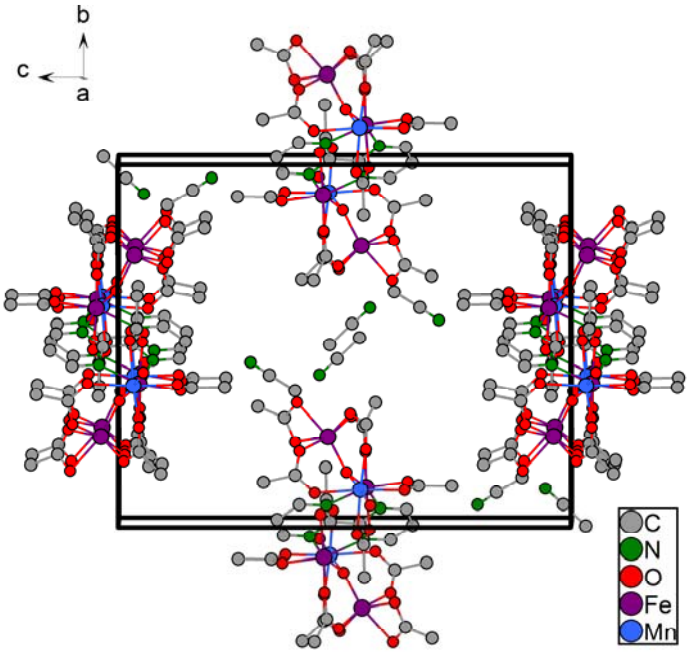

Figure S6. Crystal packing of the unit cell of complex **6**. View along the H-bond interacting chains. H atoms and *tert*-butyl groups omitted for sake of clarity.

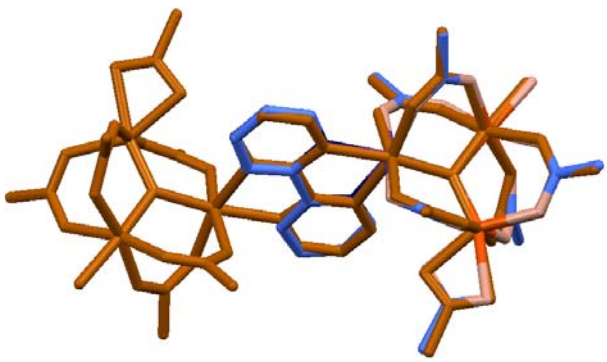

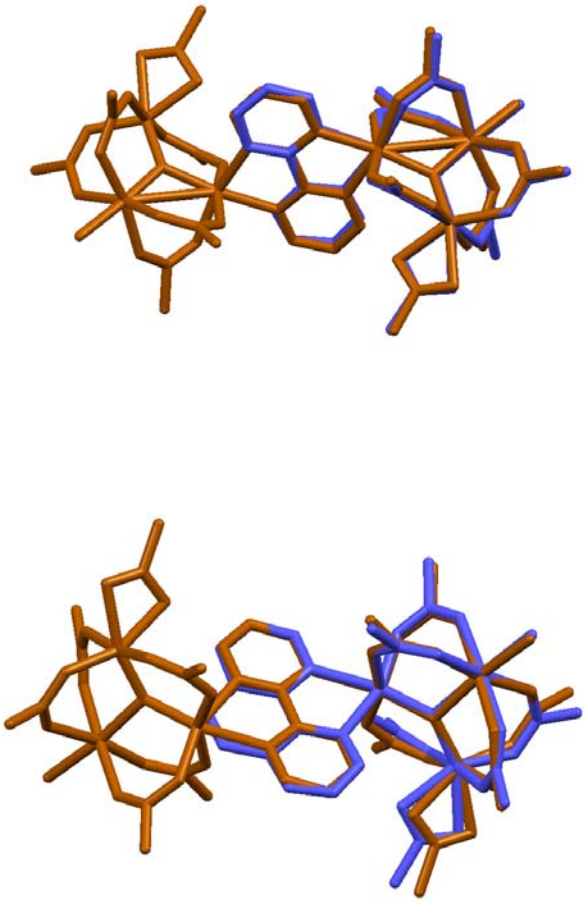

Figure S7. Overlaid X-ray structures of the pair complexes **1**-**4**, **2**-**5** and **3**-**6** (top to bottom respectively) with the rms described in the text. Blue: trinuclear complexes **1**-**3**; brown: hexanuclear complexes **4**-**6**.

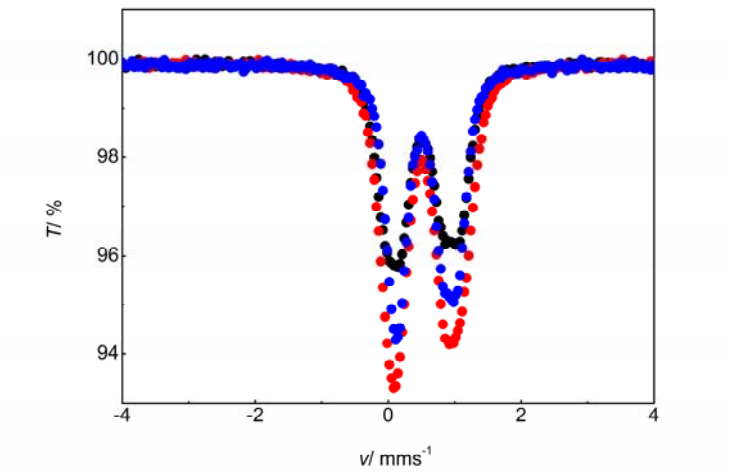

Figure S8. Overlaid Moessbauer spectra at 80K of complexes **4** (red), **5**(blue) and **6** (black).

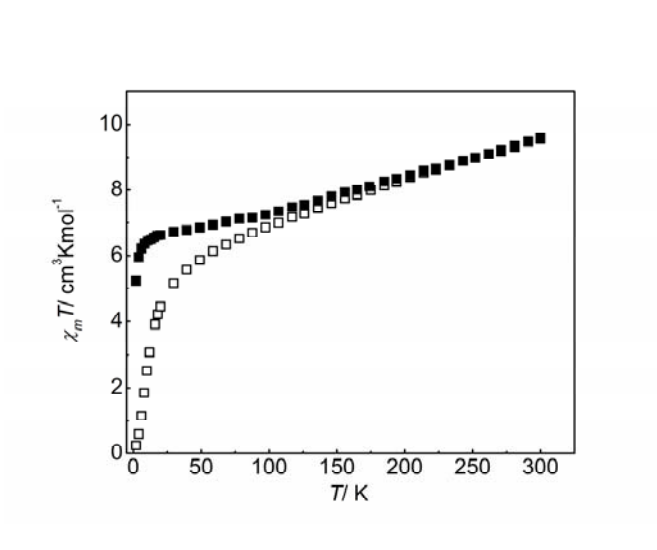

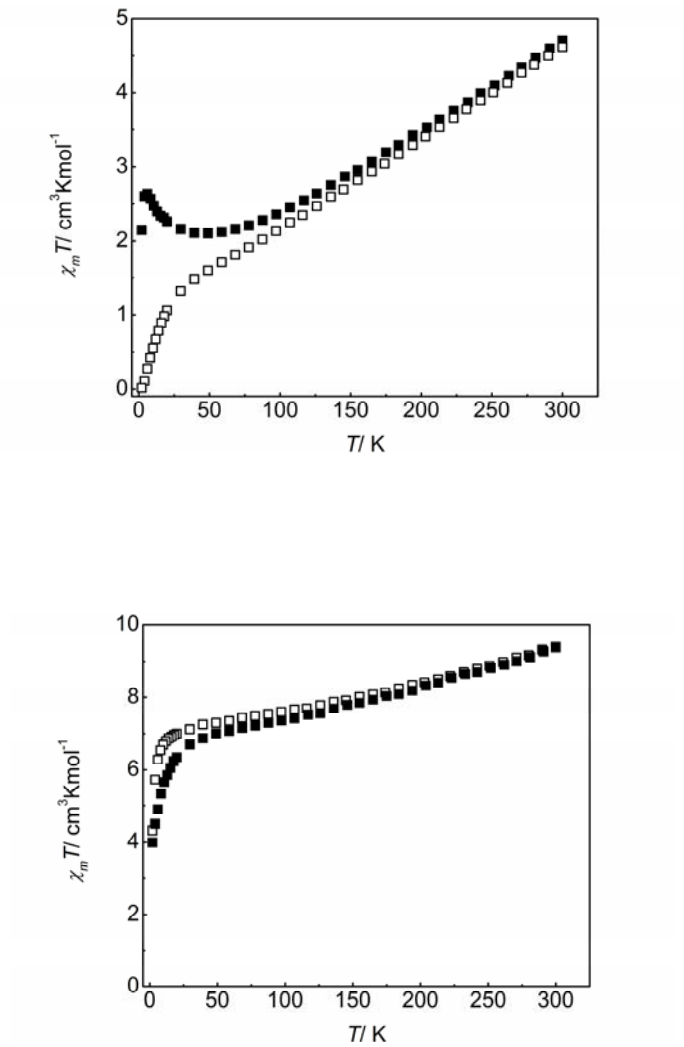

Figure S9. Overlaid $\chi_m T$ data plots of the complexes pairs **1**-**4**, **2**-**5** and **3**-**6** (top to bottom respectively). Filled squares: trinuclear complexes **1**-**3** data, multiplied by a factor two. Open squares: hexanuclear complexes **4**-**6** data.

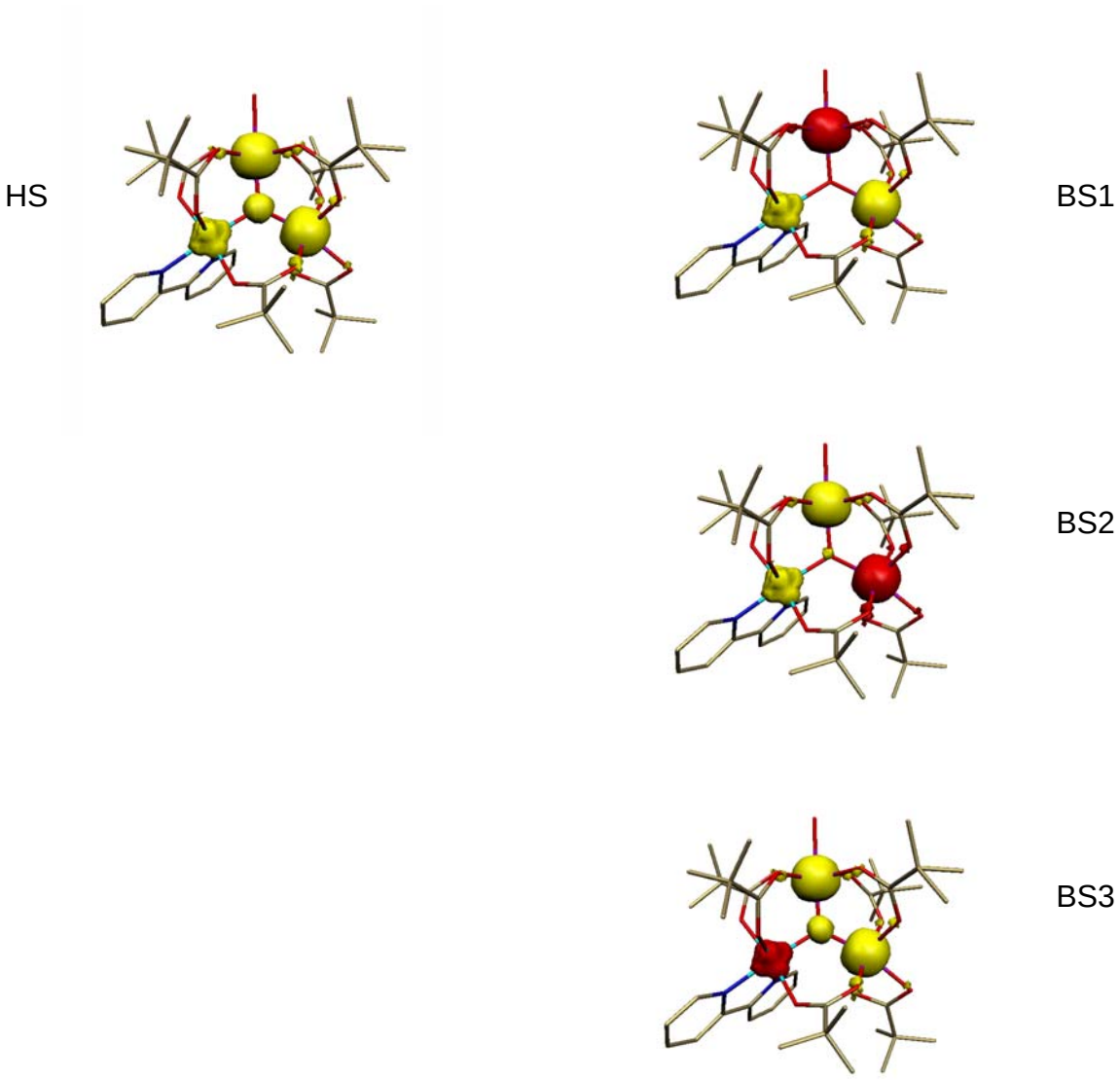

Figure S10. Spin density isosurfaces of the different spin topologies employed in the Broken-Symmetry exchange coupling constants calculations of complexes **1**-**3** (illustrated with compound **2**). Yellow: positive spin density; Red: negative spin density.

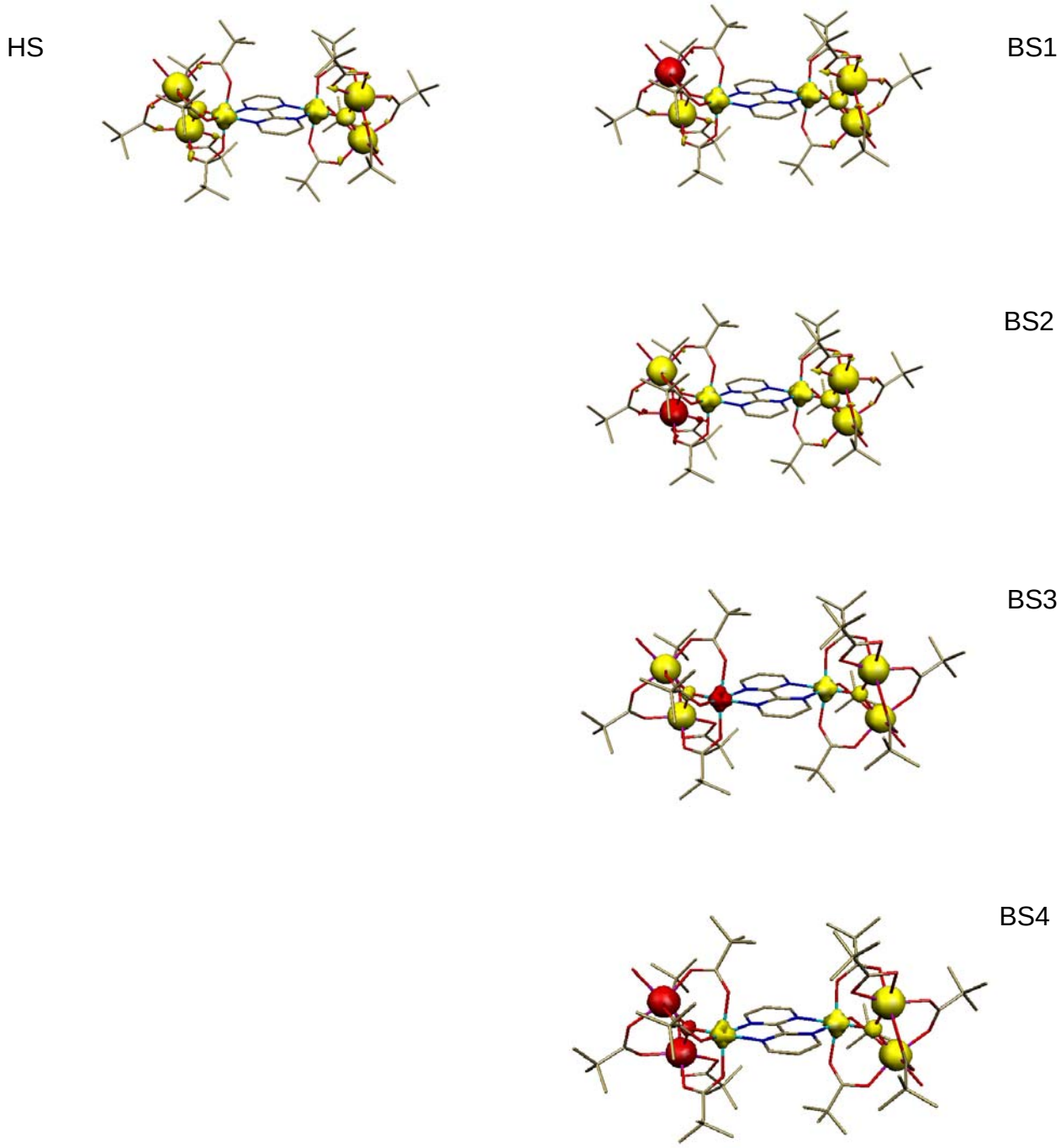

Figure S11. Spin density iso-surfaces of the different spin topologies employed in the Broken-Symmetry exchange coupling constants calculations of complexes **4**-**6** (illustrated with compound **5**). Yellow: positive spin density; Red: negative spin density.

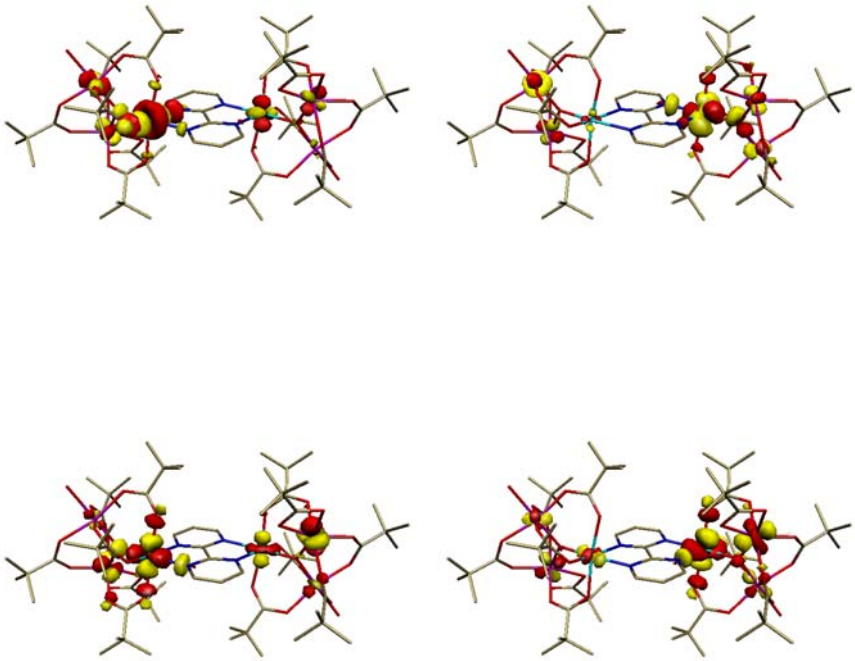

Figure S12. Natural localized orbitals pairs with unitary occupancy, centered at Co(II) sites that show σ-type exchange pathway through the bipyrimidine bridge in complex **4**.

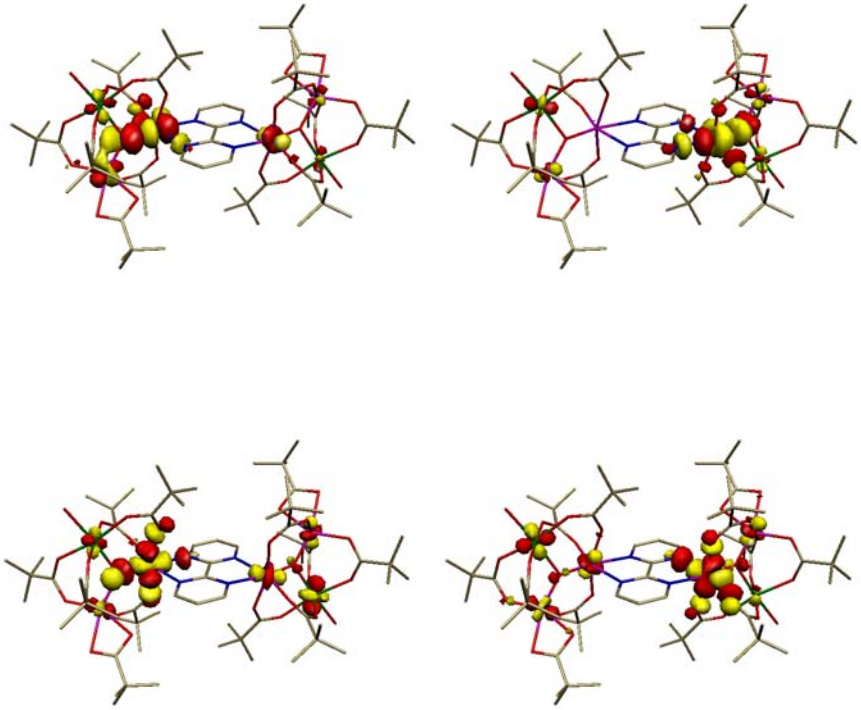

Figure S13. Natural localized orbitals pairs with unitary occupancy, centered at Fe(III) sites, that show σ-type exchange pathway through the bipyrimidine bridge in complex **6**.